Geochemistry, Geophysics, Geosystems

RESEARCH ARTICLE
10.1029/2018GC007802

Key Points:
- Water column surveys, 1985-2017, show that hydrothermal plume rise height and turbidity identify the last three Axial Seamount eruptions
- Posteruptive enhancement of hydrothermal activity lasted 2-5 years posteruption, totaling ~10 years over the survey duration
- Posteruption heat flux increased sixfold, implying that fluxes based on noneruptive activity alone will underestimate the long-term flux

Supporting Information:
- Supporting Information S1
- Figure S1
- Data Set S1
- Data Set S2
- Data Set S3
- Data Set S4

Correspondence to:
E. T. Baker,
edward.baker@noaa.gov

Citation:
Baker, E. T., Walker, S. L., Chadwick, W. W., Jr, Butterfield, D. A., Buck, N. J., & Resing, J. A. (2019). Posteruption enhancement of hydrothermal activity: A 33-year, multieruption time series at Axial Seamount (Juan de Fuca Ridge). *Geochemistry, Geophysics, Geosystems*, *20*, 814–828. https://doi.org/10.1029/2018GC007802

Received 29 JUN 2018
Accepted 27 OCT 2018
Accepted article online 21 DEC 2018
Published online 7 FEB 2019

Posteruption Enhancement of Hydrothermal Activity: A 33-Year, Multieruption Time Series at Axial Seamount (Juan de Fuca Ridge)

Edward T. Baker[1,2], Sharon L. Walker[2], William W. Chadwick Jr[3], David A. Butterfield[1,2], Nathaniel J. Buck[1,2], and Joseph A. Resing[1,2]

[1]Joint Institution for the Study of the Atmosphere and Ocean, University of Washington, Seattle, WA, USA, [2]NOAA/Pacific Marine Environmental Laboratory, Seattle, WA, USA, [3]NOAA Pacific Marine Environmental Laboratory, Newport, OR, USA

Abstract Mid-ocean ridge eruptions, initiating or revitalizing hydrothermal discharge and disrupting seafloor ecosystems, occur regularly as a consequence of plate spreading. Evaluating their impact on long-term hydrothermal discharge requires information on the scale and duration of any posteruption enhancement. Here we describe a unique hydrothermal plume time series of annual (or more frequent) observations at Axial Seamount vent fields from 1985 through 2017, missing only 7 years. Axial, a hot spot volcano astride the Juan de Fuca Ridge, experienced eruptions in 1998, 2011, and 2015. In 1998 and 2011 lava flooded the SE caldera and south rift zone, but in 2015 most lava was extruded in a series of flows extending ~20 km down the north rift zone. Response cruises occurred within 18 days (1998) to about 4 months, followed by regular posteruption observations. All 30 cruises measured plume rise height (a proxy for heat flux) and turbidity (indicative of chemical changes in vent discharge) at several vent sites, yielding an integrated view of vent field activity. Venting in the SE caldera area persisted throughout the time series, consistent with the imaged location of the shallowest portion of the melt-rich magma reservoir. Eruptions produced substantial and diagnostic increases in plume rise and turbidity, and posteruption enhancements lasted 2–5 years, totaling ~10 years over the course of the time series. Estimates of the relative heat flux indicate a sixfold increase during eruption-enhanced periods, implying that generalizations about mid-ocean ridge hydrothermal fluxes may be underestimates if based on non–eruption-enhanced hydrothermal activity alone.

Plain Language Summary We use a three-decade-long time series to understand how seafloor volcanic eruptions affect hydrothermal venting. Axial Seamount, 1,400 m deep and about 400 km off the coast of Washington state, has erupted in 1998, 2011, and 2015. Each eruption caused a substantial increase, lasting 2 to 5 years, in the discharge of hot fluids and chemicals from the seafloor. These eruption periods thus contributed more heat and chemicals to the ocean than the 20 years with no eruption activity. Seafloor eruptions may thus play a more important role in hydrothermal venting than previously expected.

1. Introduction

Submarine eruptions accelerate the transfer of heat, chemicals, and microbes from the crust to the ocean while destroying and revitalizing ecosystem habitats. Despite the profundity of these changes, information about their frequency, duration, and impacts is scarce. In the last three decades, over 35 submarine eruptions worldwide have generated a sea-going response (Baker et al., 2012; Rubin et al., 2012). About half the responses have been timely enough to confirm an eruption-induced change in hydrothermal heat or chemistry, but only 10 (8 on mid-ocean ridges and 2 on arc volcanoes) have benefited from multiple posteruption hydrothermal studies.

Posteruption physical and chemical investigations seek to understand how eruptions modify the long-term thermal and chemical characteristics of seafloor volcanic environments. For example, German and Lin (2004) proposed a conceptual mid-ocean ridge model that partitions the cumulative heat flux across several decades between eruptions: (1) heat flux released by massive hydrothermal venting (event plumes) during an eruption (providing 5% of the total flux), (2) enhanced posteruption discharge lasting a few years (20%), and (3) "normal" chronic flux persisting decades until the next eruption (75%). The authors emphasized that these temporal scales, especially eruption intervals, fundamentally depend on the

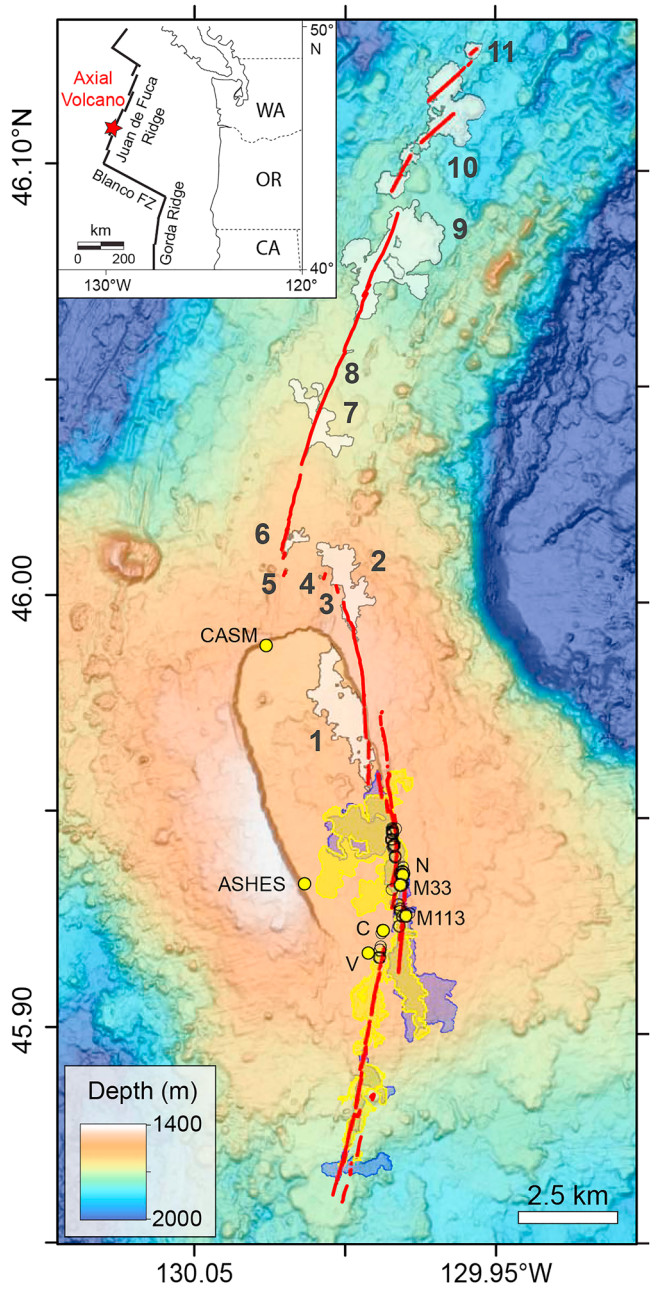

Figure 1. Bathymetry of Axial Seamount and its location in the NE Pacific Ocean. Lava flow emplacements are shown for 1998 (blue), 2011 (yellow), and 2015 (white). The 2015 flows are numbered according to Chadwick et al. (2016); flows 3, 4, 5, and 8 are very small. Mapped fissures for all eruptions (Chadwick et al., 2013; Clague et al., 2017) are shown in red. Vent sites include those named in the text (yellow dots) and the distribution of known vent sites (some now buried) along the south rift zone (black circles). Ephemeral sites associated with lava flows are not shown. Vent names: N = Nascent, M33 = Marker 33, M113 = Marker 113, C = Castle, V = Vixen. CASM = Canadian American Seamount Expedition; ASHES = Axial Seamount Hydrothermal Emissions Study.

magmatic character of a given ridge or volcano. On some intermediate- and fast-spreading ridges (Clague et al., 2013; Embley et al., 2000; Fornari et al., 2012), eruptions have occurred on the decadal scale or less.

A crucial aspect of the German and Lin (2004) model is the duration and heat flux of the enhanced hydrothermal discharge interval, which determines the relative proportions of heat supplied during eruption-enhanced and nonenhanced chronic venting on mid-ocean ridges. Several studies, on the spatial scales of both vent field (Baker et al., 1998; Massoth et al., 1994) and vent orifices (Fornari et al., 2012; Lilley et al., 2003; Oosting & Von Damm, 1996; Von Damm, 2004), document eruption-induced changes lasting 1–5 years. Less is known about heat flux changes following an eruption, but short time series following the 1993 CoAxial (Baker et al., 1998) and 1998 Axial Seamount (Baker et al., 2004) eruptions found that posteruption heat flux decayed as $\sim time^{-1}$.

Gauging the impact of episodic events is challenging. Progress advances as monitoring programs lengthen, but decadal-scale monitoring has been rare. Here we describe a unique water column data set that includes hydrothermal plumes observed on the summit of Axial Seamount on 30 cruises between 1985 and 2017; only 7 years lack data, all but one before 1997 (supporting information Data Set S1 and Figure S1). A previous study followed the decline of hydrothermal venting for 3 years after the 1998 eruption (Baker et al., 2004). This paper adds to that time series and similarly follows the hydrothermal effects of the 2011 and 2015 eruptions, which have not been reported elsewhere. Using plume measurements, rather than sampling at a few individual vent orifices, allows us to assess hydrothermal fluctuations at the spatial scale of the south rift zone venting area (Figure 1). We then describe the pattern of eruption-enhanced venting over three decades, quantitatively estimating its contribution to the total heat flux. Finally, we discuss how the distribution of melt below the summit of Axial Seamount might explain the differing hydrothermal response to each of the three historical eruptions.

2. Geologic Setting

Axial Seamount straddles the intersection of the Cobb hot spot and the Juan de Fuca Ridge in the NE Pacific Ocean. The summit rises some 1,000 m above the surrounding seafloor to a minimum depth of ~1,400 m, crowned by an 8 × 3-km horseshoe-shaped caldera (Embley et al., 1990). Investigations into hydrothermal activity in the caldera gained specific targets in the early 1980s with the discovery of the Canadian American Seamount Expedition (CASM, 1985) and Axial Seamount Hydrothermal Emissions Study (ASHES) (ASHES Expedition, 1986) vent sites (Figure 1). Systematic surveys using towed instruments to map the distribution of hydrothermal plumes began in 1985 (Baker et al., 1990). Hydroacoustic monitoring detected frequent earthquake swarms following the availability of Navy sonar data in 1991 (Dziak & Fox, 1999a), now replaced by real-time monitoring using the Cabled Array of the National Science Foundation's Ocean Observatory Initiative (OOI) (Kelley et al., 2014).

Hydroacoustic, seismic, and seafloor monitoring efforts have documented three summit eruptions at Axial Seamount since 1980. The first confirmed eruption, detected by U.S. Navy hydrophones (Dziak & Fox, 1999b), began on 25 January 1998 and was monitored in situ by Bottom Pressure Recorders (Fox, 1999; Fox et al., 2001) and moorings with temperature sensors (Baker et al., 1999). It remains the only deep-sea eruption where water column moorings recorded the

initiation of enhanced hydrothermal venting concurrent with the onset of seismicity and lava emplacement. Earthquake epicenters showed that a dike propagated 50 km down the south rift zone from the summit (Dziak & Fox, 1999b). However, lava flows were erupted only on 11 km of the upper south rift zone in and near the SE corner of the caldera (Figure 1), with maximum thickness of 26 m and a total volume of 0.024 km^3 (Chadwick et al., 2013; Clague et al., 2017; Embley et al., 1999).

Remotely operated vehicle (ROV) dives discovered the next eruption in July 2011; later examination of Bottom Pressure Recorder and Ocean Bottom Hydrophone data determined the eruption date as 6 April 2011 (Chadwick et al., 2012; Dziak et al., 2012). Lava flows covered roughly the same portion of the SE caldera as in 1998 (45.87°N to 45.95°N), and likely used some of the same eruptive fissures (Caress et al., 2012; Clague et al., 2017; Figure 1). Lava flows emplaced on the upper SE rift zone totaled 0.034 km^3 with a maximum thickness of 29 m, remarkably similar to the 1998 eruption (Clague et al., 2017). Unlike 1998, however, a large hummocky pillow ridge was erupted on the lower south rift zone, ~30 km south of the caldera, with a maximum flow thickness of 167 m and a volume of 0.060 km^3, for a total erupted volume in 2011 of ~0.94 km^3 (Caress et al., 2012; Clague et al., 2017).

The latest eruption began on 24 April 2015 and was the first to be detected and monitored (except for a complete absence of water column plume sensors) by the OOI Cabled Array (Chadwick et al., 2016; Nooner & Chadwick, 2016; Wilcock et al., 2016, 2018). This eruption was the first known to emplace lava flows on the north rift zone since Axial Seamount monitoring and mapping began in the 1980s. Inside the caldera, a single flow flooded the NE side as far south as ~45.95°N. This flow, with a maximum thickness of ~13 m, totaled 0.008 km^3, about one third to one quarter of the 1998 and 2011 volumes erupted inside the caldera. Ten additional flows (Figure 1) were erupted on the northeastern caldera rim and along 14.5 km of the north rift, totaling 0.15 km^3 with a maximum thickness of 128 m near the north end terminus (Chadwick et al., 2016; Clague et al., 2017).

Before 2015, the only active hydrothermal vents observed north of 45.95°N along the eastern wall of the caldera or the north rift zone were diffuse fields on the rift zone near 46.0386°N, 130.0124°W. Since the early 1980s, >100 named vent structures or areas, many buried by lava flows after their discovery, have been located along the upper south rift zone between 45.95°N and 45.915°N (Figure 1). The only other known active areas not associated with the southeastern caldera wall and rift zone are ASHES and CASM, near the west and north caldera walls, respectively.

3. Methods

For all ship-based hydrothermal plume mapping we used a *SeaBird 911plus* (or earlier models) conductivity-temperature-depth (CTD) package with a turbidity sensor. From 1985 to 1992 the turbidity sensor was a Sea Tec 0.25 m transmissometer. For most subsequent years we used first Sea Tec, followed by Seapoint, light-backscattering sensors. Exceptions include 2005–2006 and 2010–2013 when only a WET Labs C-Star 401DR transmissometer was available. All light transmission data were converted to backscattering data by comparing instruments on multiple casts (supporting information Figure S2). A chemical sensor (oxidation-reduction potential) was also used in 2011, 2015, and 2017.

Light-backscattering values (nondimensional Nephelometric Turbidity Units [NTU]; American Public Health Association, 1985) indicate particle-rich discharge, generally at temperatures > ~ 250 °C, with copious black smoker metal oxides or sulfur-rich minerals that create plumes extending many kilometers from their source. The notation ΔNTU indicates the NTU value (0–5 V range on the sensor corresponds to a 0–5 NTU range) in excess of the background value observed in the local ambient water. The oxidation-reduction potential sensor detects hydrothermal discharge at all temperatures. It responds immediately to the presence of nanomolar (and greater) concentrations of reduced hydrothermal chemicals (e.g., Fe^{2+}, HS^-, and H_2) with a sharp decrease in potential values (E [mV]), followed by a much slower recovery (Baker et al., 2016; Walker et al., 2007). These plume chemicals are out of equilibrium with the oxidizing ocean (Resing et al., 2009) and rapidly oxidize or metabolize close to their seafloor source, based on a ~1-day half-life for Fe^{+2} oxidation (Massoth et al., 1998). Abrupt decreases in E as small as 0.5 mV can indicate a hydrothermal plume.

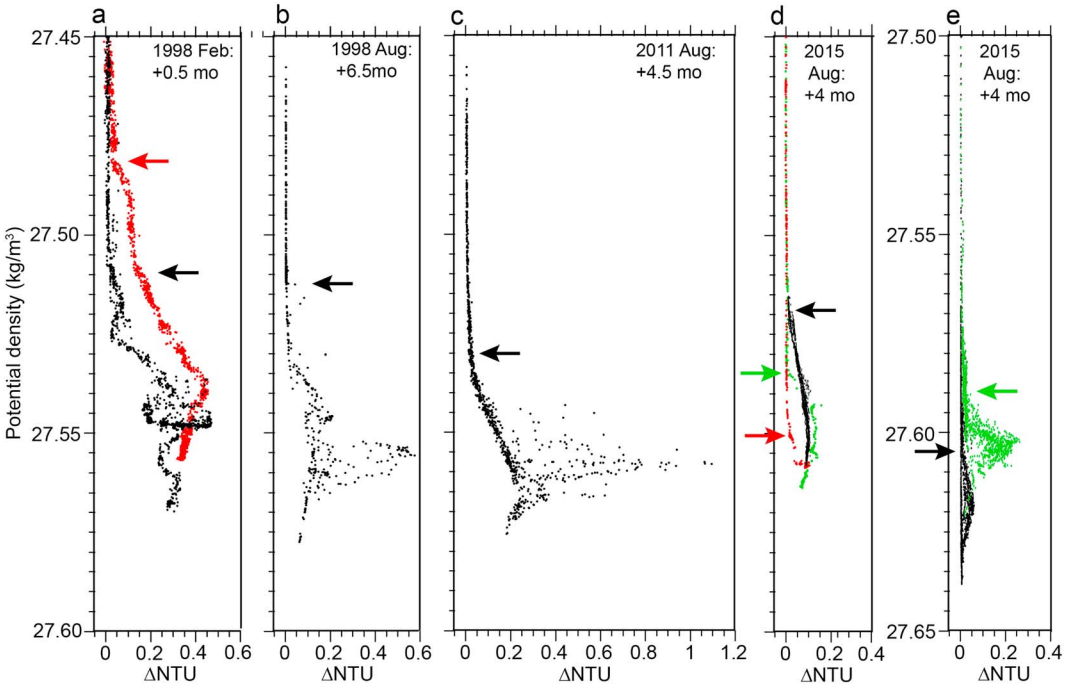

Figure 2. Plume profiles of turbidity (ΔNTU) versus potential density (σ_θ), extending to the seafloor over newly erupted lava after an eruption. Color-coded horizontal arrows mark plume tops. (a) At 18 days posteruption in 1998. Black line is a plume (V16) near the eruption site. Red line is the maximum plume rise observed (V7), which occurred west of the caldera in a plume apparently sourced at the eruption site (i.e., σ_θ = 27.570 kg/m^3). (b) At 6.5 months after the 1998 eruption. (c) At 4.5 months after the 2011 eruption. (d) At 4 months after the 2015 eruption in the caldera. Black profile is CTD T15A02 along the base of the northeastern wall of the caldera (as far south as 45.95°N). Red and green profiles are from casts over vent fields on the south rift zone (Castle, 45.9262°N, and Vixen, 45.9173°N, respectively), not over the 2015 flow. (e) At 4 months after the 2015 eruption over lava flows 9 (green) and 10 (black; see Figure 1) on the north rift zone (note scale change on the σ_θ axis due to deeper depth). CTD = conductivity-temperature-depth.

Hydrothermal temperature anomalies (Δθ°C) were calculated as in the past for Axial Seamount (Baker et al., 2004):

$$\Delta\theta = \theta - (m_0 + m_1\sigma_\theta + m_2\sigma_\theta)$$

where σ_θ is potential density and m_0, m_1, and m_2 are constants in a linear or polynomial regression between σ_θ and θ in hydrothermally unaffected waters around the plume. The Δθ values reported here for all years have been increased by a factor of 2.1 using standard hydrographic corrections and assuming vent discharge salinities equal to the local seawater, following McDougall (1990) and Lavelle et al. (1998).

The rise height of a hydrothermal plume is a function of the near-bottom density stratification, the discharge heat flux, and the horizontal current flow (Morton et al., 1956). Temporal variability of the local density stratification can thus change rise height for even a steady heat flux. Xu and Lavelle (2017), using a numerical model of ocean flow, hydrography, and transport averaged over 29.5-day periods, find that the depth of any given isopycnal near Axial Seamount can vary temporally by up to 80 m between the caldera and the adjacent flank (within the ~1,350- to 1,500-m-depth interval). The model further shows that tidal currents and internal waves create vertical water currents of up to 3 cm/s near the caldera walls, also degrading the value of using rise height to accurately estimate heat flux. Because of these confounding factors, we use the potential density interval ($\Delta\sigma_\theta$), instead of the depth interval, between the seafloor and plume top to track temporal changes in plume rise height, and thus (approximately) heat flux, from venting areas (Figure 1). We define the plume top as the shallowest isopycnal where plume ΔNTU or ΔE become negligible (Figure 2); this definition also corresponds to the depth at which the vertical velocity of the rising plume ceases (Turner, 1973). Substantial variation in horizontal currents can also lower rise height by bending the plume (Lavelle, 1997) and may introduce some cruise-to-cruise variability in $\Delta\sigma_\theta$.

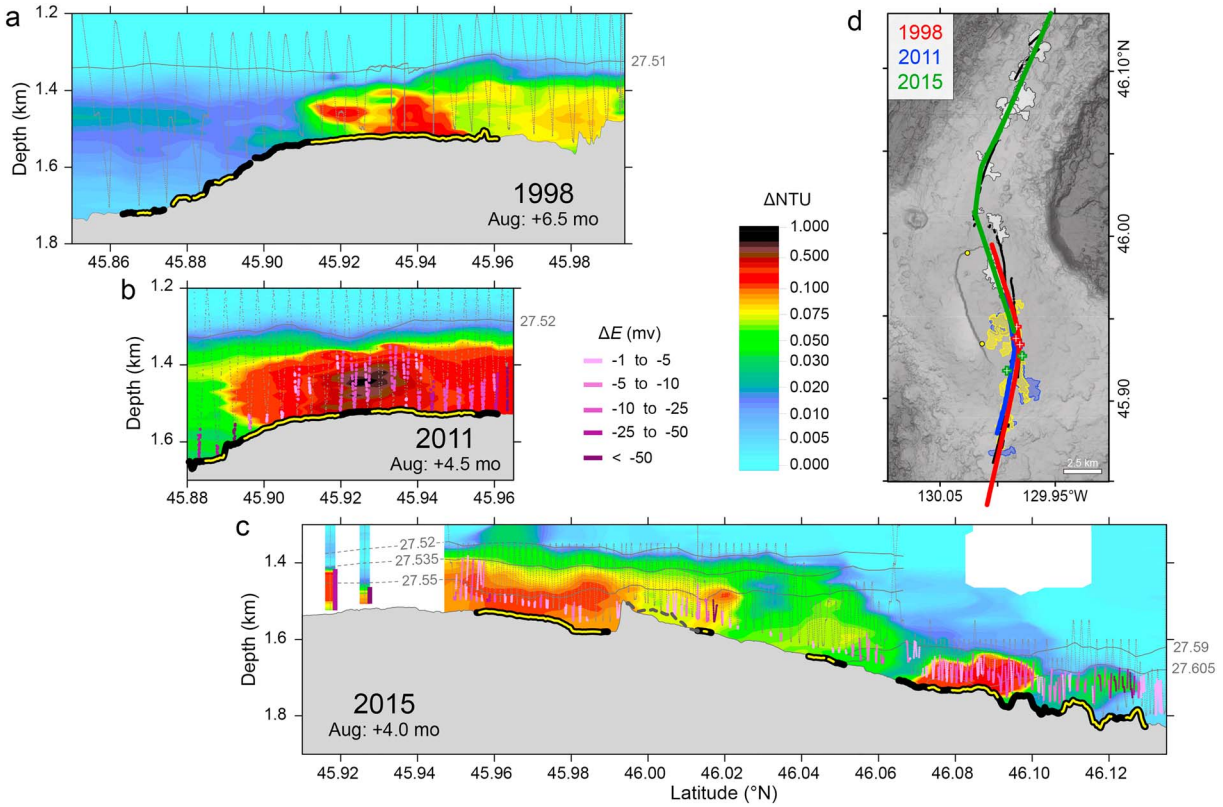

Figure 3. Posteruption hydrothermal plumes over Axial Seamount. Plume rise was similar 4–6.5 months after each event. Plumes contoured in ΔNTU, with Δ*E* overlain on conductivity-temperature-depth (CTD) paths. Thick black lines on profile bathymetry indicate the extent of new lava flows; yellow lines indicate where the CTD was directly over the flows. (a) August 1998 along the southeast rift of the caldera. (b) August 2011 along the same track as in 1998. (c) August 2015 from midcaldera (along the eastern wall) to 46.13°N on the north rift zone. Plumes at sites near the 1998 and 2011 eruptions shown by vertical profiles near 45.92°N. (d) Plan view map of the flows and CTD tow paths. Black lines show fissure locations (see also Figure 1).

The *Sentry* Autonomous Underwater Vehicle (AUV) conducted extensive near-bottom (65-m altitude) multibeam sonar mapping surveys over some of the 2015 lava flows in both 2015 (dives 336–341) and 2017 (dives 442–446). The surveys were combinations of dense grids (160-m line spacing) for high-resolution bathymetric mapping and sparser tracklines inside and outside the caldera to document seafloor depth changes due to volcanic deformation (Caress et al., 2016; Clague et al., 2017). On each dive, a Miniature Autonomous Plume Recorder mounted on *Sentry* collected NTU, *E*, temperature, and pressure data every 5 s. In 2017 there was only a single grid bathymetric survey, east of the north rift zone and away from any known 2015 lava flow, and four dives for deformation monitoring. No NTU or *E* data are available from AUV surveys following the 2011 eruption.

4. Eruption-Induced Hydrothermal Plume Data

4.1. The 1998 Eruption

The 1998 eruption underwent the most rapid and detailed water column response of any ridge crest eruption (Baker et al., 1999, 2004; Cowen et al., 1999; Feely et al., 1999; Lupton et al., 1999; McLaughlin-West et al., 1999; Resing et al., 1999). It remains the only such event where three-dimensional monitoring instruments (i.e., including the water column) were in place before, during, and after an eruption. Only lacking were AUV surveys for high-resolution mapping of hydrothermal discharge from the cooling lava flows. Because the first response cruise arrived just 18 days after the eruption started (RV *Wecoma* cruise W9802), it was the only Axial Seamount eruption where event-plume-type discharge, rising at least 300 m ($\Delta\sigma_\theta$ = 0.092 kg/m^3) above the eruption site, was observed (Figure 2a). Both $\Delta\sigma_\theta$ (0.067 kg/m^3) and maximum ΔNTU (ΔNTU_{max}, 0.5–0.6) values remained strongly elevated during a subsequent cruise 6.5 months posteruption along the upper south rift zone (Figures 2b and 3a). ΔNTU > ~0.2 normally indicates high

concentrations of eruption-associated particulate (elemental) S, especially in snowblower discharge rich in bacterial material (Crowell et al., 2008; Feely et al., 1999), which has a much higher effective scattering ratio than mineral particles (Baker et al., 2001). Particulate S exceeded preeruption concentrations by a factor of ~1,000 (Feely et al., 1999), and H_2S/heat (nmol/J) from a south rift zone vent (Marker 33) increased by a factor of 10 (Butterfield et al., 2004). Six months also approximates the interval over which both particulate S/heat (nmol/J; Baker et al., 1998) and vent fluid H_2S/heat (Butterfield et al., 1997) increased several folds following the 1993 eruption at the CoAxial Floc vent field, Juan de Fuca Ridge.

4.2. The 2011 Eruption

The first hydrothermal plume survey of the upper south rift zone after the 2011 event occurred ~4 months posteruption on two cruises: AT18-08 (http://www.rvdata.us/catalog/AT18-08) and TN268 (http://www.rvdata.us/catalog/TN268). The plume distribution was remarkably similar to that ~6.5 months after the 1998 event (Figures 2c and 3b). A single tow (CTD-09) and two casts (CTDs 13, 14) along the south rift zone during TN268 found a plume centered near 45.93°N, where maximum $\Delta\sigma_\theta$ was slightly lower (0.047 kg/m^3) than in 1998 and ΔNTU_{max} (1.1) was the highest ever recorded at Axial Seamount. ROV transects found unusually murky water everywhere in the caldera, attributed to many more snowblower vents than just the six visually documented (http://www.rvdata.us/catalog/TN268). Analysis of snowblower material found high concentrations of the sulfur oxidizing bacteria *Epsilonproteobacteria* and sulfur concentrations up to 38% by weight (Meyer et al., 2013), again implicating particulate S in creating extraordinarily high ΔNTU plume values.

4.3. The 2015 Eruption

4.3.1. Neutrally Buoyant Plumes

As in 2011, no plume surveys occurred until ~4 months after the 2015 eruption. A response cruise in August 2015 (http://www.rvdata.us/catalog/TN327) thoroughly mapped plumes along the eastern wall of the caldera (as far south as 45.95°N) and the north rift zone with CTD tow-yos, and within the near-bottom waters over most of the major lava flows with AUV *Sentry* (Figures 2d, 2e, 3c, and 4a). Notably, the caldera wall tow (T15A02) provided the first evidence for active venting north of 45.95°N along the eastern wall, where some of the 2015 eruptive fissures were located.

In the caldera, above flow 1 (Figure 1; here and elsewhere we use the numbering scheme published in Chadwick et al., 2016), tow T15A02 (Figures 2d and 3c) found a maximum $\Delta\sigma_\theta$ of 0.04 kg/m^3 and a ΔNTU_{max} of 0.13, both lower, and ΔNTU_{max} markedly so, than either of the previous eruptions in the caldera. A low ΔNTU_{max} implies a weaker S discharge than in 1998 and 2011, corresponding to ROV surveys that were unable to locate any discrete venting sites associated with the very thin flow 1 (13 m maximum; Chadwick et al., 2016). Conversely, $\Delta\theta$ values in the plume maxima equaled the 0.08 °C value typical of both the 1998 and 2011 events at similar posteruption times, and ΔE anomalies confirmed venting sites in the southern half of flow 1 (Figure 3c).

ΔE profiles, which, unlike ΔNTU and $\Delta\theta$, strongly respond to venting only close (on the order of a few kilometers) to the sensor, can be used to determine which parts of the caldera were hydrothermally affected by the eruption. Over flow 1, the elevated $\Delta\sigma_\theta$ (0.04 kg/m^3) was identical whether using the vertical extent of ΔNTU or ΔE profiles. To the south (Castle [V15A04] and Vixen [V15A02]; Figure 1), $\Delta\sigma_\theta$ was lower using either ΔNTU or ΔE. But at ASHES (V15A03), the $\Delta\sigma_\theta$ value calculated using the vertical extent of ΔNTU was 0.05 kg/m^3, ~10 times higher than from ΔE, indicating that an older, higher-rising plume from the north end of the caldera had penetrated at least as far south and west as ASHES, but not to Vixen or Castle. Thus, the southern half of the caldera apparently experienced no 2015 eruption impact that lasted >4 months; an absence of observable changes in diffuse sites there supports this conclusion (http://www.rvdata.us/catalog/TN327).

Along the north rift zone, CTD tows T15A01/04 (Figures 2e and 3c) found the highest ΔE (180 mV) and ΔNTU_{max} (0.25) values above the three most northerly and thickest (maximum thickness 67–128 m) lava flows (9–11). Maximum $\Delta\sigma_\theta$ here reached 0.03 kg/m^3. $\Delta\theta$ values reached a maximum of ~0.15 °C above flow 10 and point to widespread and vigorous venting. ROV surveys (Chadwick et al., 2016; http://www.rvdata.us/catalog/TN327) observed extensive diffuse hydrothermal flow on the thick 2015 lava flows on the north rift zone. Some vents were already colonized by tubeworms, and locally thick microbial mats completely

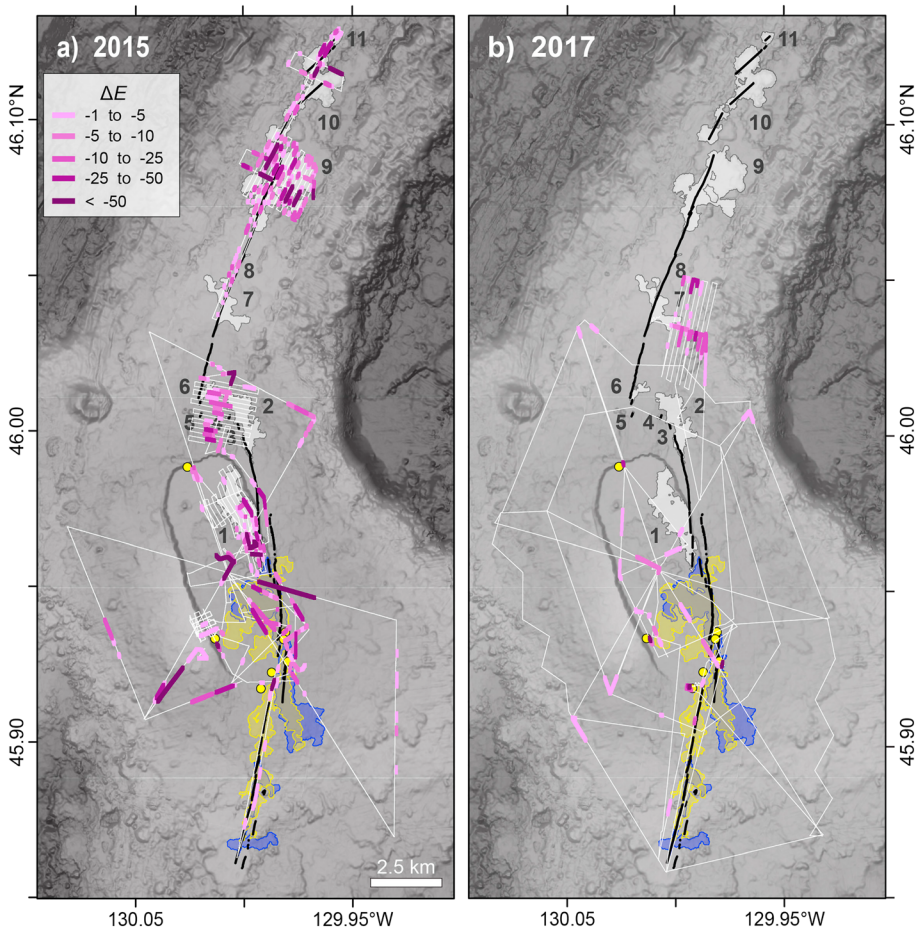

Figure 4. Near-bottom Δ*E* data from (a) August 2015 and (b) August 2017 along *Sentry* paths (white lines) at 65 m above bottom. Lava flows shown for 1998 (blue), 2011 (yellow), and 2015 (white); fissures (black lines); and vent sites as in Figure 1.

covered the surfaces of the new flows (Chadwick et al., 2016). However, unlike the caldera eruption in 2011, only a single snowblower vent, on flow 9, was seen on the north rift flows. Interestingly, differences in the plumes above the two most voluminous flows, 9 (67 m maximum thickness) and 10 (128 m maximum thickness), imply significant differences in the chemistry of their seafloor discharge. ΔNTU_{max} values were 4 times higher over flow 9 than flow 10 (0.25 vs. 0.06), and $\Delta NTU_{max}/\Delta\theta$ ratios were about double (1.37 ± 0.44 vs. 0.67 ± 0.14). Conversely, Δ*E* values were highest over flow 10. Differences were also found in the microbial populations sampled in the two plumes (Spietz et al., 2018). Enhanced ΔNTU is suggestive of elevated particulate S, though limited vent fluid sampling (only four sites on flows 9 and 10) found no evidence of high H_2S concentrations. These flows stand in sharp contrast to the up to 114-m-thick 1996 Gorda Ridge flow (Chadwick et al., 1998; Yeo et al., 2013), which produced only weak plumes (~0.02 °C) 1 month after the eruption (Baker, 1998) and nearly undetectable plumes at 6 months (Massoth et al., 1998).

4.3.2. Near-Bottom Plumes

The 2015 eruption was the first to be comprehensively mapped (seafloor and water column plume sensing) by an AUV while the emplaced lava still generated warm discharge (Chadwick et al., 2016; Figure 4a). Seismic monitoring and geologic mapping indicate that the eruption included either two dikes (Wilcock et al., 2016) or a single left-stepping dike (Chadwick et al., 2016) that began below the eastern caldera wall, surfaced beneath flow 1, and then propagated northward along the north rift zone. Near-bottom data from *Sentry* (supporting information Data Set S3) mapped the hydrothermal impacts of these dikes (Figure 4a).

Intense ΔE values were present throughout the footprints of the thick (67- to 128-m maximum) northern flows (9–11), even 4 months posteruption. Conversely, ΔE anomalies nearer to the caldera (flows 2–8) more closely follow the path of rift zone fissures created by the dike (Chadwick et al., 2016; Clague et al., 2017), indicating that these thinner flows, all with maximum thicknesses <20 m, had already largely cooled. These data agree with ROV observations of widespread diffuse discharge on the northern, but not the southern, lava flows (Chadwick et al., 2016).

Wide-ranging *Sentry* surveys for deformation monitoring also discovered near-bottom plumes 1–3 km beyond the caldera footprint, not associated with lava flows, mostly in the SW quadrant (Figure 4a). We propose that these plumes originated in the caldera, then advected clockwise around the summit as described by the model results of Xu and Lavelle (2017). Their model predicts that after 1 day, a period during which ΔE would be expected to remain detectable (based on a ~1-day half-life for Fe^{+2} oxidation; Massoth et al., 1998), a tracer from ASHES would occupy the SW quadrant of the summit to a radius of ~5 km from ASHES. Thus, plumes to the SW could originate anywhere in the caldera. Baker et al. (2004) described analogous plume fragments, identified by $\Delta\theta$ anomalies and observed west of the caldera as far north as 45.983 °C, 6 months after the 1998 eruption. One exception to this pattern is the group of ΔE anomalies on the south rift zone between 1,570 and 1,611 m (~45.885°N). These plumes are deeper than sources in the caldera (< ~1,540 m), which suggest a still active location of weak venting. An anomaly in this area was also detected in 2017.

4.3.3. The 2017 Observations

Unfortunately, almost 2 years passed before plume surveys were performed again in July 2017 (http://www.rvdata.us/catalog/RR1712). Casts at Castle (V17A01) and Vixen (V17A02) along the south rift found typical noneruption values of both $\Delta\sigma_\theta$ (<0.013 kg/m^3) and ΔNTU_{max} (<0.07), but no cast was made over the 2015 NE caldera flow. A single cast (V17A03) on flow 11 at 46.12°N found no hydrothermal evidence, though an ROV survey found active venting from small chimneys near the CTD cast location. *Sentry* mapping inside and near the caldera found anomalies over CASM, ASHES, and the upper south rift zone but not over flows 2–6 (Figure 4b and supporting information Data Set S4). A gridded *Sentry* bathymetric survey partially over and east of flow 7, ~1 km east of a 2015 ΔE rift signal, recorded multiple ΔE and ΔNTU anomalies in each of two locations ~1.5 km apart. This result is consistent with weak sources still active on the upper north rift zone.

4.4. Eruption Enhancement of Chronic Venting

4.4.1. Eruption Patterns

The ability of seafloor eruptions to create or enhance chronic hydrothermal venting has been demonstrated repeatedly (Baker, 1998; Baker et al., 1987, 1998, 1999, 2011; Cowen et al., 2007; Fornari et al., 2012). Thus, changes in plume rise and physical/chemical characteristics should be expected from eruptions, but lengthy (decades) and regular (annual) time series observations of hydrothermal activity on the seafloor and in the water column are available only from Axial Seamount. Because plumes spread widely and ΔNTU values degrade slowly, using plumes to monitor temporal changes in vent-field-scale activity can be more practical and effective than monitoring individual vent orifices. To visualize the effect of an eruption on chronic venting, we plot plume $\Delta\sigma_\theta$ and ΔNTU_{max} for 30 cruises spanning 1985 to 2017 (Figure 5). Plume observations have been concentrated along the upper south rift zone and include 11 cruises with tow data and 18 cruises with vertical CTD casts only (supporting information Data Set S1 and Figure S1). For 2015, we also use plume data from the northern half of the eastern caldera wall and the north rift zone. Observations at ASHES (except for 1987 and 1988 when no other data were available) and CASM are not included because of sparser sampling and uncertainty in distinguishing the ASHES plume from the typically westward advecting plumes from the south rift zone. For each cruise, we plot the largest observed $\Delta\sigma_\theta$ and ΔNTU_{max}.

This unprecedented 33-year time series identifies the three historical eruptions and finds no evidence for undetected eruptions equivalent in scale to the known ones (although the time series prior to 1997 is incomplete). We categorize plumes as eruption enhanced when $\Delta\sigma_\theta \geq 0.04$ kg/m^3 and/or $\Delta NTU_{max} \geq 0.2$. In 2015, $\Delta\sigma_\theta$ reached 0.04 kg/m^3 only in the caldera (although $\Delta\sigma_\theta$ for plumes over rift flows 9 and 10 [>0.03 kg/m^3] was much higher than for non–eruption-enhanced caldera plumes), whereas ΔNTU_{max} exceeded 0.2 only over flow 9 on north rift zone. These categories define three intervals of posteruption enhancement

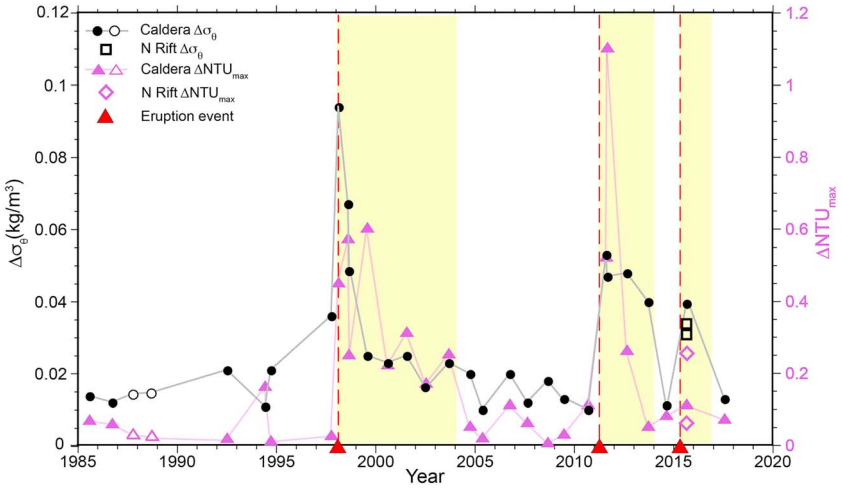

Figure 5. Time series of plume rise ($\Delta\sigma_\theta$ [kg/m^3]) and plume maximum ΔNTU (ΔNTU_{max}) within the caldera and, for 2015, the north rift zone (lava flows 9 and 10). Solid circles and triangles are data from the upper south rift zone and, for 2015, the base of the northeastern caldera wall; open circles and triangles are from ASHES vent field; open squares and diamonds are 2015 flows 9 and 10 from the north rift zone. Solid red triangles and dashed lines mark eruptions, and yellow bands span the inferred duration of eruption-enhanced venting. Variability of $\Delta\sigma_\theta$ outside of eruption-enhanced periods may result from current-induced plume bending. ASHES = Axial Seamount Hydrothermal Emissions Study.

(Figure 5), where mean $\Delta\sigma_\theta = 0.037 \pm 0.016$ kg/m^3 and mean $\Delta NTU_{max} = 0.347 \pm 0.264$ are significantly higher (at P levels <0.01) than the means of all other years ($\Delta\sigma_\theta = 0.020 \pm 0.020$ kg/m^3 and $\Delta NTU_{max} = 0.075 \pm 0.101$).

The posteruption enhanced periods varied greatly among the three historical eruptions. Eighteen months after the 1998 eruption, $\Delta\sigma_\theta$ had declined to non–eruption-enhanced levels (0.025 kg/m^3), whereas ΔNTU_{max} remained high before slowly decreasing, from 2001 to 2004, to non–eruption-enhanced values (< ~0.1). Posteruption enhancement of chronic venting lasted at least ~5.5 years after the 1998 event, extending by ~2 years the time series described in Baker et al. (2004). The 2011 eruption followed a contrasting pattern, where elevated $\Delta\sigma_\theta$ values remained stable for at least 2.5 years while a rapidly declining ΔNTU_{max} returned to non–eruption-enhanced levels in the same time interval. Even shorter was the 2015 enhancement. $\Delta\sigma_\theta$ and ΔNTU_{max} were at non–eruption-enhanced levels 2.2 years after the eruption and perhaps earlier given the absence of any observations in 2016. Thus, our 33-year time series shows that chronic venting was enhanced for as much as approximately one third of the time, as evidenced by posteruption increases in $\Delta\sigma_\theta$ and/or ΔNTU_{max}.

Using the time series data, we can estimate the relative contribution of posteruption enhanced discharge to the total heat flux from the southeast rift zone of Axial Seamount since 1985. We begin with the simplifying assumption that plumes from the southeast rift zone represent the output of a single point source with chloride concentrations equal to seawater. This simplification acknowledges that we know precisely neither the number nor the chemistry of active discrete discharge sources in any year. Next, we calculate a proxy heat flux (H_p) for each time series point using the relationship $H_p = (c_p\rho/\alpha g)(z_{max}/3.8)^4N^3$, where c_p is heat capacity for neutrally buoyant plume water at ~150 bar (4,100 J/(kg°C); Bischoff & Rosenbauer, 1985), ρ is the local plume fluid density (1,028 kg/m^3), α is the thermal expansion coefficient (~1.3×10^{-4} °C^{-1}; McDuff, 1995), g is gravitational acceleration (9.8 m/s^2), z_{max} is plume rise, and N is the local Brunt-Väisälä frequency ($[(-g\Delta\rho)(\rho\Delta z)^{1/2}]$, 1.91×10^{-3} Hz). This heat flux formulation has origins in Morton et al. (1956) and is clearly expressed for hydrothermal plumes in, for example, Campbell et al. (1984) and Little et al. (1987). More recently, Carazzo et al. (2008) have shown that because this standard formulation assumes a constant entrainment coefficient as a plume rises, it underestimates the true H. Application of their revised formulation to plumes above the Trans-Atlantic Geotraverse field on the Mid-Atlantic Ridge yielded H values about 3 times greater than originally calculated by Rudnicki and Elderfield (1992). However, because $H \propto (z_{max})^4$, small differences in z_{max} cause substantial changes in H, lessening the influence of variability in other

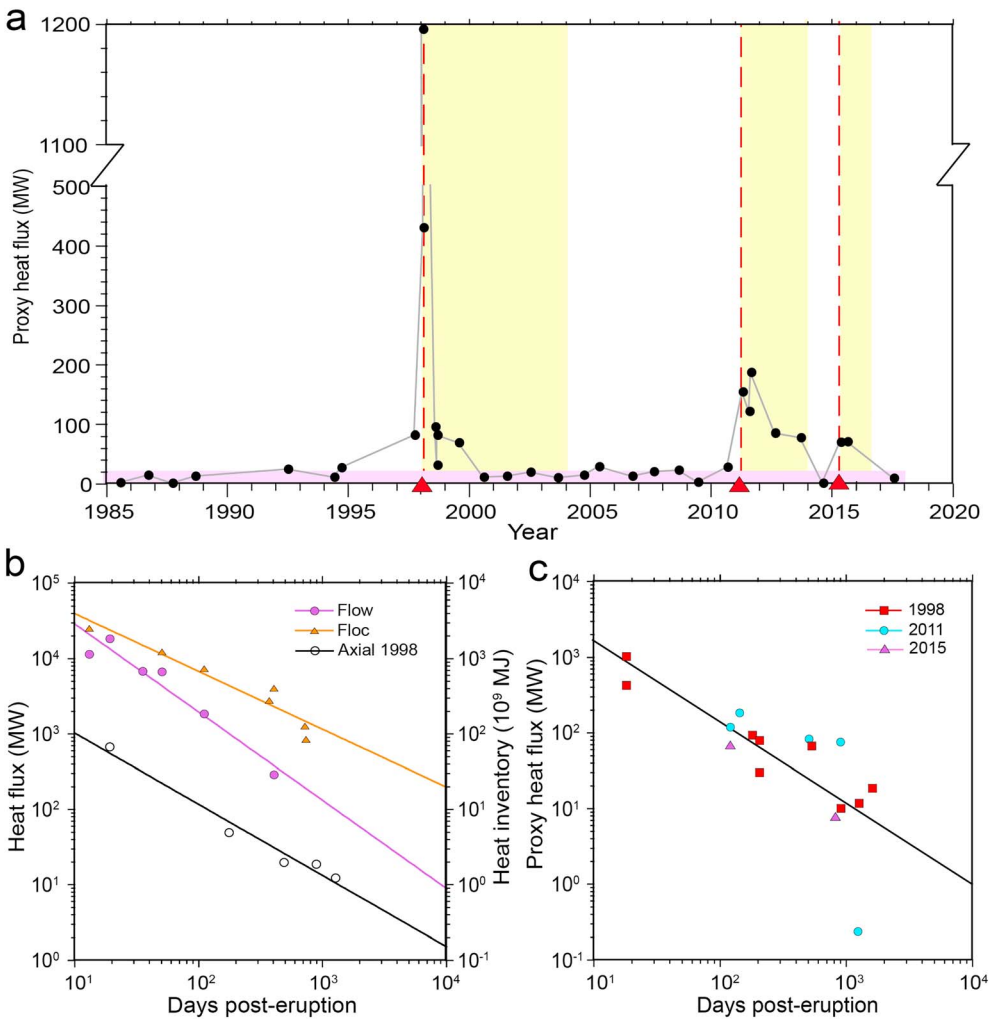

Figure 6. (a) Proxy heat flux (MW) time series based on plume rise (converted to meters) from Figure 5. Note break on *y* axis. Yellow bands show intervals of posteruption enhancement from Figure 5. Pink band shows "normal" chronic heat flux averaging ~15 MW. Total time series discharge estimated as 45 GJ, total above background (i.e., eruption enhanced) estimated at 30 GJ; relative numbers only. (b) Posteruption decay from measured heat fluxes at two different vent fields after the 1993 CoAxial eruption (Baker et al., 1998), and from heat inventory measurements following the 1998 Axial eruption (Baker et al., 2004). Decay slopes are $time^{-1.2}$ ($r = 0.78$; Flow field), $time^{-0.8}$ ($r = 0.98$; Floc field), and $time^{-0.9}$ ($r = 0.99$; Axial). (c) Comparative plot based on proxy heat flux values in (a). Combined data from the three Axial eruptions show a decay of $time^{-1.1}$ ($r = 0.87$).

constants. Because we are interested only in the temporal variability of H_p, and because of the extreme variability in H measurements at individual hydrothermal sites regardless of the method used (e.g., Baker, 2007; Ramondenc et al., 2006), we here report only H_p values using the constant entrainment formulation.

For z_{max}, we take the height of the plume corresponding to the $\Delta\sigma_\theta$ value for each data point in Figure 5 (not considering those for the 2015 north rift zone plumes). We next integrate the resultant H_p curve (Figure 6), first over the entire time series ($\sum$45 GJ) and then again after removing the eruption-enhanced intervals to calculate a noneruption background ($\sum$15 GJ). By subtracting this background from the entire time series, we find that of the total heat discharged during the time series, about two thirds ($\sum$30 GJ) occurred by means of increased (above background) H_p during eruption-enhanced periods lasting only one third of the time series. Overall, H_p during the eruption-enhanced periods averaged about 6 times higher (97 MW) than outside those periods (15 MW). These results give quantitative context to the German and Lin (2004) model and lead to the conclusion that generalizations about mid-ocean ridge hydrothermal fluxes may be considerable

underestimates if based on noneruptive hydrothermal activity alone. An interesting exception to this conclusion is CO_2; at Axial Seamount, CO_2 ratios are relatively constant even during eruption-enhanced venting (Butterfield & Lilley, 2018).

Published values of H for chronic (non–eruption enhanced) venting at Axial Seamount are 15–75 MW for ASHES alone (Rona & Trivett, 1992) and 800 MW for the entire summit area (Baker et al., 1990). Our H_p values likely underestimate the true H because we assume only a single source produces the observed plume, even though many sources are active (Figure 1).

Although the absolute magnitudes of our calculated H_p values are uncertain, the similarity of our trends in posteruption H_p decay to other studies of posteruption heat decay supports our quantitative interpretations. Measured H observed following the 1993 CoAxial eruption (Baker et al., 1998) and comprehensive heat inventories at Axial Seamount from 1998 to 2001 (Baker et al., 2004) decayed as $\sim time^{-1}$ (Figure 6b), as did our combined posteruption H_p observations at Axial Seamount (Figure 6c). The figures further suggest that the absence of comprehensive plume data during the first ~2 weeks after any eruption leads to a substantial underestimate of posteruption enhancement. For example, sensors on caldera moorings during the 1998 Axial eruption show that in situ temperatures 100 m above bottom increased from 2.4 to 2.85 °C within hours of lava eruption. Temperatures gradually declined to 2.5 °C over the 18 days before the first response cruise, then remained roughly constant over the next 6 months (Baker et al., 1999). Thus, the period of highly increased plume temperatures, and presumably increased heat fluxes, ended before plume surveys even commenced.

Recovery periods of ~2–5 years agree with other estimates based on monitoring plumes or vent chemistry at other eruption sites. Plumes generated by the 1993 CoAxial eruption returned to background in 1 and 2 years at the Flow and Floc sites, respectively (Baker et al., 1998). On the East Pacific Rise near 9°N, the chlorinity of fluids from Bio 9, P, and F vents recovered in 3–5 years from eruption-induced freshening in 1992 and 2006 (Fornari et al., 2012; Oosting & Von Damm, 1996; Von Damm, 2004), whereas vent chemistry in the Endeavour field underwent no more than a yearlong change after an intrusive event in 1999 (Lilley et al., 2003).

4.4.2. Connections to Axial Seamount Geology

How well can we correlate hydrothermal enhancement with the volcanic characteristics of each eruption? Heat supply from cooling dikes and lava flows has stimulated venting throughout the caldera and rift zones during the three eruptions, but only the southeast corner of the caldera has a continuous record of hydrothermal venting. For dike cooling, models (e.g., Cherkaoui et al., 1997; Lowell & Xu, 2000) and observations (e.g., Coogan et al., 2005) indicate that the time span of a dike alone to power high-temperature venting is typically on the order of a year or less. This time scale is consistent with our observations, 4 months posteruption in 2015, of widespread discharge along the dike path as defined by the north rift zone fissures and the east caldera wall.

Lava flows likely support venting for even shorter times. Field examples of the rapid cooling of pillow lavas include the Flow site at CoAxial (up to 30 m thick; Chadwick et al., 1995; Embley et al., 2000) and the 1996 Gorda Ridge eruption (up to 114 m thick; Chadwick et al., 1998; Yeo et al., 2013). In both cases, plume $\Delta\theta$ had declined to ~0.02 °C by 1–3 months posteruption (Baker, 1998; Baker et al., 1998). At Axial Seamount, the thin (<20 m) 2015 flows (1–8) showed scant evidence of discharge except directly over the rift zone, whereas the thicker (67–128 m) flows (9–11) showed widespread hydrothermal plume anomalies remaining 4 months after the eruption. We attribute that relative longevity to their massive volume (~0.13 km^3), ~3 to 8 times greater than at Gorda Ridge (0.054 km^3) or CoAxial (0.018 km^3).

We conclude that the 1998 and 2011 events produced more long-lasting and robust caldera plumes because they overlie the shallowest and highest melt portion of the summit magma reservoir as imaged by multichannel seismic surveys (Arnulf et al., 2014). The northern half of the caldera, in contrast, largely overlays the deeper and lower-melt/higher-mush portion of the magma reservoir, perhaps explaining (along with limited exploration) its lack of observed venting until 2015. Further, the absence of any imaged magma reservoir north of ~46.02°N implies that the heat source for the 2015 north rift plumes was restricted to the intruded dike and erupted lava flows, incapable of sustaining a robust hydrothermal field.

5. Conclusions

A 33-year time series of hydrothermal plumes on the summit of Axial Seamount shows that eruptions in 1998, 2011, and 2015 markedly increased plume rise and turbidity. The 2015 eruption was notable in two ways. It was the first historical eruption in the northern half of the caldera, which had no previous record of venting except at CASM. It also provided the first observations of extensive venting along the north rift zone. The persistence of summit venting (focused in the SE portion of the caldera), compared to the sparsity of venting in the northern caldera and rapid decline of venting on the north rift zone after the 2015 eruption, is consistent with recent seismic observations of shallow magma with high melt content beneath the southern caldera, deeper magma with more crystal mush farther north, and an absence of melt beneath the north rift zone.

Enhanced posteruption venting lasted 2–5 years after each eruption, totaling approximately 10 years. Plume rise, measured in terms of the potential density interval from seafloor to plume top, averaged 0.039 ± 0.021 kg/m^3 during the 10 years of posteruption enhancement compared to 0.017 ± 0.008 kg/m^3 in other years, evidence of an eruption-increased heat flux. Similarly, posteruption turbidity (measured by light backscattering) varied from 0.365 ± 0.286 during posteruption enhancement intervals to 0.053 ± 0.043 ΔNTU in other years, likely due to increased discharge of sulfur particles following eruptions. Estimated heat flux increases were also substantial during the posteruption periods, averaging about 6 times the normal chronic flux. Even this increase may be artificially low, due to the absence of plume data during the first weeks of each eruption. Generalizations about mid-ocean ridge hydrothermal fluxes may be considerable underestimates if based only on noneruptive hydrothermal activity.

Data from the OOI Cabled Array provided copious and unique information on crustal processes during the 2015 eruption but virtually none on the hydrothermal response because of the absence of water column instrumentation. Event plumes are hallmarks of mid-ocean ridge eruptions but have yet to be confirmed at Axial Seamount because of the lack of plume data from the first days posteruption. Adding water column moorings and resident mobile platforms (e.g., AUVs and gliders; Manalang & Delaney, 2016; Wilcock et al., 2018) to the Cabled Array would accelerate studies of crustal-ocean interactions and allow the Axial node of the Ocean Observatory to truly observe the ocean.

Acknowledgments
We thank the Woods Hole Oceanographic Institution Sentry team for expert support during our cruises in 2015 and 2017, J.W. Lavelle for insightful comments on the manuscript, and the many scientists and ships that maintained this time series. This research was supported by the NOAA/PMEL Earth-Ocean Interactions and Vents Programs, the Cooperative Institute for Marine Resources Studies (CIMRS), and the Joint Institute for the Study of the Atmosphere and Ocean (JISAO) under NOAA Cooperative Agreements NA11OAR4320091 and NA10OAR4320148. Ship time for CTD operations at Axial Seamount between 2007 and 2017 was supported by National Science Foundation awards OCE-0725605, 1155849, 1356839, and 1546616, and by NOAA/PMEL. The authors declare no financial conflicts. Previously unpublished data used in this paper, or their repository sources, are found in the supporting information. This paper is PMEL contribution 4792 and JISAO contribution 2018-0153.

References

American Public Health Association (1985). Standard methods for the examination of water and wastewater, 16th Ed. Washington, DC: A.P.H.A., A.W.W.A, and W.P.C.F. 1268.

Arnulf, A. F., Harding, A. J., Kent, G. M., Carbotte, S. M., Canales, J. P., & Nedimović, M. R. (2014). Anatomy of an active submarine volcano. *Geology*, *42*(8), 655–658. https://doi.org/10.1130/G35629.1

ASHES Expedition (1986). Pisces submersible exploration of a high-temperature vent field in the caldera of Axial Volcano, Juan de Fuca Ridge. *Eos, Transactions American Geophysical Union*, *67*, 1027.

Baker, E. T. (1998). Patterns of event and chronic hydrothermal venting following a magmatic intrusion: New perspectives from the 1996 Gorda Ridge eruption. *Deep Sea Research, Part II*, *45*(12), 2599–2618. https://doi.org/10.1016/S0967-0645(98)00085-X

Baker, E. T. (2007). Hydrothermal cooling of midocean ridge axes: Do measured and modeled heat fluxes agree? *Earth and Planetary Science Letters*, *263*(1-2), 140–150. https://doi.org/10.1016/j.epsl.2007.09.010

Baker, E. T., Chadwick, W. W. Jr., Cowen, J. P., Dziak, R. P., Rubin, K. H., & Fornari, D. J. (2012). Hydrothermal discharge during submarine eruptions: The importance of detection, response, and new technology. *Oceanography*, *25*(1), 128–141. https://doi.org/10.5670/oceanog.2012.11

Baker, E. T., Fox, C. G., & Cowen, J. P. (1999). In situ observations of the onset of hydrothermal discharge during the 1998 submarine eruption of Axial Volcano, Juan de Fuca Ridge. *Geophysical Research Letters*, *26*, 3445–3448. https://doi.org/10.1029/1999GL002331

Baker, E. T., Lowell, R. P., Resing, J. A., Feely, R. A., Embley, R. W., Massoth, G. J., & Walker, S. L. (2004). Decay of hydrothermal output following the 1998 seafloor eruption at Axial Volcano: Observations and models. *Journal of Geophysical Research*, *109*, B01205. https://doi.org/10.1029/2003JB002618

Baker, E. T., Lupton, J. E., Resing, J. A., Baumberger, T., Lilley, M., Walker, S. L., & Rubin, K. (2011). Unique event plumes from a 2008 eruption on the Northeast Lau Spreading Center. *Geochemistry, Geophysics, Geosystems*, *12*, Q0AF02. https://doi.org/10.1029/2011GC003725

Baker, E. T., Massoth, G. J., & Feely, R. A. (1987). Cataclysmic hydrothermal venting on the Juan de Fuca Ridge. *Nature*, *329*(6135), 149–151. https://doi.org/10.1038/329149a0

Baker, E. T., Massoth, G. J., Feely, R. A., Cannon, G. A., & Thomson, R. E. (1998). The rise and fall of the CoAxial hydrothermal site, 1993–1996. *Journal of Geophysical Research*, *103*, 9791–9806. https://doi.org/10.1029/97JB03112

Baker, E. T., McDuff, R. E., & Massoth, G. J. (1990). Hydrothermal venting from the summit of a ridge-axis seamount: Axial Volcano, Juan de Fuca Ridge. *Journal of Geophysical Research*, *95*, 12,843–12,854. https://doi.org/10.1029/JB095iB08p12843

Baker, E. T., Resing, J. A., Haymon, R. M., Tunnicliffe, V., Lavelle, W., Martinez, F., & Nakamura, K. (2016). How many vent fields? New estimates of vent field populations on ocean ridges from precise mapping of hydrothermal discharge locations. *Earth and Planetary Science Letters*, *449*, 186–196. https://doi.org/10.1016/j.epsl.2016.05.031

Baker, E. T., Tennant, D. A., Feely, R. A., Lebon, G. T., & Walker, S. L. (2001). Field and laboratory studies on the effect of particle size and composition on optical backscattering measurements in hydrothermal plumes. *Deep Sea Research*, *48*(2), 593–604. https://doi.org/10.1016/S0967-0637(00)00011-X

Bischoff, J. L., & Rosenbauer, R. J. (1985). An empirical equation of state for hydrothermal seawater (3.2 percent NaCl). *American Journal of Science*, *285*(8), 725–763. https://doi.org/10.2475/ajs.285.8.725

Butterfield, D. A., Jonasson, I. R., Massoth, G. J., Feely, R. A., Roe, K. K., Embley, R. E., et al. (1997). Seafloor eruptions and evolution of hydrothermal fluid chemistry. *Philosophical Transactions of the Royal Society of London A: Mathematical, Physical and Engineering Sciences*, *355*(1723), 369–386.

Butterfield, D. A., & Lilley, M. D. (2018). Tracking salt and magmatic gas in two hydrothermal observatories in the NE Pacific, Abstract V52B-03 presented at 2018 fall meeting, AGU, Washington, D.C., 10-14 Dec.

Butterfield, D. A., Roe, K. K., Lilley, M. D., Huber, J. A., Baross, J. A., Embley, R. W., & Massoth, G. J. (2004). Mixing, reaction and microbial activity in the sub-seafloor revealed by temporal and spatial variation in diffuse flow vents at Axial Volcano. In W. S. D. Wilcock, D. Kelley, E. F. DeLong, & S. C. Cary (Eds.), *The subseafloor biosphere at mid-ocean ridges*, *Geophysical Monograph Series*, (Vol. 144, pp. 269–289). Washington, DC: American Geophysical Union.

Campbell, I. H., McDougall, T. J., & Turner, J. S. (1984). A note on fluid dynamic processes which can influence the deposition of massive sulfides. *Economic Geology*, *79*(8), 1905–1913. https://doi.org/10.2113/gsecongeo.79.8.1905

Canadian American Seamount Expedition (1985). Hydrothermal vents on an axis seamount of the Juan de Fuca Ridge. *Nature*, *313*(5999), 212–214. https://doi.org/10.1038/313212a0

Carazzo, G., Kaminski, E., & Tait, S. (2008). On the rise of turbulent plumes: Quantitative effects of variable entrainment for submarine hydrothermal vents, terrestrial and extra terrestrial explosive volcanism. *Journal of Geophysical Research*, *113*, B09201. https://doi.org/10.1029/2007JB005458

Caress, D. W., Clague, D. A., Paduan, J. B., Martin, J. F., Dreyer, B. M., Chadwick, W. W. Jr., et al. (2012). Repeat bathymetric surveys at 1-metre resolution of lava flows erupted at Axial Seamount in April 2011. *Nature Geoscience*, *5*(7), 483–488. https://doi.org/10.1038/ngeo1496

Caress, D. W., Clague, D. A., Paduan, J. B., Thomas, H. J., Chadwick, W. W., Jr., Nooner, S. L., & Yoerger, D. R. (2016). Vertical deformation of the Axial Seamount summit from repeated 1-m scale bathymetry surveys using AUVs. Abstract OS41C-1991 presented at 2016 Fall Meeting, AGU, San Francisco, CA.

Chadwick, W. W. Jr., Clague, D. A., Embley, R. W., Perfit, M. R., Butterfield, D. A., Caress, D. W., et al. (2013). The 1998 eruption of Axial Seamount: New insights on submarine lava flow emplacement from high-resolution mapping. *Geochemistry, Geophysics, Geosystems*, *14*, 3939–3968. https://doi.org/10.1002/ggge.20202

Chadwick, W. W. Jr., Embley, R. W., & Fox, C. G. (1995). SeaBeam depth changes associated with recent lava flows, CoAxial segment, Juan de Fuca Ridge: Evidence for multiple eruptions between 1981–1993. *Geophysical Research Letters*, *22*, 167–170. https://doi.org/10.1029/94GL01895

Chadwick, W. W. Jr., Embley, R. W., & Shank, T. M. (1998). The 1996 Gorda Ridge eruption: Geologic mapping, sidescan sonar, and SeaBeam comparison results. *Deep Sea Research, Part II*, *45*(12), 2547–2569. https://doi.org/10.1016/S0967-0645(98)00083-6

Chadwick, W. W. Jr., Nooner, S. L., Butterfield, D. A., & Lilley, M. D. (2012). Seafloor deformation and forecasts of the April 2011 eruption at Axial Seamount. *Nature Geoscience*, *5*(7), 474–477. https://doi.org/10.1038/ngeo1464

Chadwick, W. W. Jr., Paduan, J. B., Clague, D. A., Dreyer, B. M., Merle, S. G., Bobbitt, A. M., et al. (2016). Voluminous eruption from a zoned magma body after an increase in supply rate at Axial Seamount. *Geophysical Research Letters*, *43*, 12,063–12,070. https://doi.org/10.1002/2016GL071327

Cherkaoui, A. S. M., Wilcock, W. S. D., & Baker, E. T. (1997). Thermal fluxes associated with the 1993 diking event on the CoAxial segment, Juan de Fuca Ridge: A model for the convective cooling of the dike. *Journal of Geophysical Research*, *102*, 24,887–24,902. https://doi.org/10.1029/97JB02123

Clague, D. A., Dreyer, B. M., Paduan, J. B., Martin, J. F., Chadwick, W. W. Jr., Caress, D. W., et al. (2013). Geologic history of the summit of Axial Seamount, Juan de Fuca Ridge. *Geochemistry, Geophysics, Geosystems*, *14*, 4403–4443. https://doi.org/10.1002/ggge.20240

Clague, D. A., Paduan, J. B., Caress, D. W., Chadwick, W. W. Jr., Le Saout, M., Dreyer, B., & Portner, R. (2017). High-resolution AUV mapping and targeted ROV observations of three historical lava flows at Axial Seamount. *Oceanography*, *30*(4), 82–99. https://doi.org/10.5670/oceanog.2017.426

Coogan, L. A., Kasemann, S. A., & Chakraborty, S. (2005). Rates of hydrothermal cooling of new oceanic upper crust derived from lithium-geospeedometry. *Earth and Planetary Science Letters*, *240*(2), 415–424. https://doi.org/10.1016/j.epsl.2005.09.020

Cowen, J. P., Glazer, B., Fornari, D. J., Shank, T. M., Soule, S. A., et al., et al. (2007). Volcanic eruptions at East Pacific Rise near 9 50′N. *Eos, Transactions American Geophysical Union*, *88*(7), 81–83. https://doi.org/10.1029/2007EO070001

Cowen, J. P., Shackelford, R., McGee, D., Lam, P., Baker, E. T., & Olson, E. (1999). Microbial biomass in the hydrothermal plumes associated with the 1998 Axial Volcano eruption. *Geophysical Research Letters*, *26*, 3637–3640. https://doi.org/10.1029/1999GL002343

Crowell, B. W., Lowell, R. P., & Von Damm, K. L. (2008). A model for the production of sulfur floc and "snowblower" events at mid-ocean ridges. *Geochemistry, Geophysics, Geosystems*, *9*, Q10T02. https://doi.org/10.1029/2008GC002103

Dziak, R. P., & Fox, C. G. (1999a). Long-term seismicity and ground deformation at Axial Volcano, Juan de Fuca Ridge. *Geophysical Research Letters*, *26*, 3641–3644. https://doi.org/10.1029/1999GL002326

Dziak, R. P., & Fox, C. G. (1999b). The January 1998 earthquake swarm at Axial Volcano, Juan de Fuca Ridge: Hydroacoustic evidence of seafloor volcanic activity. *Geophysical Research Letters*, *26*, 3429–3432. https://doi.org/10.1029/1999GL002332

Dziak, R. P., Haxel, J. H., Bohnenstiehl, D. R., Chadwick, W. W. Jr., Nooner, S. L., Fowler, M. J., et al. (2012). Seismic precursors and magma ascent before the April 2011 eruption at Axial Seamount. *Nature Geoscience*, *5*(7), 478–482. https://doi.org/10.1038/ngeo1490

Embley, R. W., Chadwick, W. W. Jr., Clague, D., & Stakes, D. (1999). The 1998 eruption of Axial Volcano: Multibeam anomalies and seafloor observations. *Geophysical Research Letters*, *26*, 3425–3428. https://doi.org/10.1029/1999GL002328

Embley, R. W., Chadwick, W. W., Perfit, M. R., Smith, M. C., & Delaney, J. R. (2000). Recent eruptions on the CoAxial segment of the Juan de Fuca Ridge: Implications for mid-ocean ridge accretion processes. *Journal of Geophysical Research*, *105*, 16,501–16,525. https://doi.org/10.1029/2000JB900030

Embley, R. W., Murphy, K. M., & Fox, C. G. (1990). High-resolution studies of the summit of Axial Volcano. *Journal of Geophysical Research*, *95*, 12,785–12,812. https://doi.org/10.1029/JB095iB08p12785

Feely, R. A., Baker, E. T., Lebon, G. T., Gendron, J. F., Resing, J. A., & Cowen, J. P. (1999). Evidence for sulfur enrichment in hydrothermal particles at Axial Volcano following the January, 1998 eruption. *Geophysical Research Letters*, *26*, 3649–3652. https://doi.org/10.1029/1999GL002325

Fornari, D. J., Von Damm, K. L., Bryce, J. G., Cowen, J. P., Ferrini, V., Fundis, A., et al. (2012). The East Pacific Rise between 9°N and 10°N: Twenty-five years of integrated, multidisciplinary oceanic spreading center studies. *Oceanography*, *25*(1), 18–43. https://doi.org/10.5670/oceanog.2012.02

Fox, C. G. (1999). In situ ground deformation measurements from the summit of Axial Volcano during the 1998 volcanic episode. *Geophysical Research Letters*, *26*, 3437–3440. https://doi.org/10.1029/1999GL900491

Fox, C. G., Chadwick, W. W. Jr., & Embley, R. W. (2001). Direct observation of a submarine volcanic eruption from a sea-floor instrument caught in a lava flow. *Nature*, *412*(6848), 727–729. https://doi.org/10.1038/35089066

German, C. R., & Lin, J. (2004). The thermal structure of the oceanic crust, ridge-spreading and hydrothermal circulation: How well do we understand their inter-connections? In *Mid-ocean ridges: Hydrothermal interactions between the lithosphere and oceans*, *Geophysical Monograph Series*, (Vol. 148, pp. 1–18). Washington, DC: American Geophysical Union. https://doi.org/10.1029/148GM01

Kelley, D. S., Delaney, J. R., & Juniper, S. K. (2014). Establishing a new era of submarine volcanic observatories: Cabling Axial Seamount and the Endeavour segment of the Juan de Fuca Ridge. *Marine Geology*, *352*, 426–450. https://doi.org/10.1016/j.margeo.2014.03.010

Lavelle, J. W. (1997). Buoyancy-driven plumes in rotating, stratified cross flows: Plume dependence on rotation, turbulent mixing, and cross-flow strength. *Journal of Geophysical Research*, *102*, 3405–3420. https://doi.org/10.1029/96JC03601

Lavelle, J. W., Baker, E. T., & Massoth, G. J. (1998). On the calculation of total heat, salt, and tracer fluxes from ocean hydrothermal events. *Deep Sea Research, Part II*, *45*(12), 2619–2636. https://doi.org/10.1016/S0967-0645(98)00086-1

Lilley, M. D., Butterfield, D. A., Lupton, J. E., & Olson, E. J. (2003). Magmatic events can produce rapid changes in hydrothermal vent chemistry. *Nature*, *422*(6934), 878–881. https://doi.org/10.1038/nature01569

Little, S. A., Stolzenbach, K. D., & Von Herzen, R. P. (1987). Measurements of plume flow from a hydrothermal vent field. *Journal of Geophysical Research*, *92*, 2587–2596. https://doi.org/10.1029/JB092iB03p02587

Lowell, R. P., & Xu, W. (2000). Sub-critical two-phase seawater convection near a dike. *Earth and Planetary Science Letters*, *174*(3–4), 385–396. https://doi.org/10.1016/S0012-821X(99)00275-7

Lupton, J. E., Baker, E., Embley, R., Greene, R., & Evans, L. (1999). Anomalous helium and heat signatures associated with the 1998 Axial Volcano event, Juan de Fuca Ridge. *Geophysical Research Letters*, *26*, 3449–3452. https://doi.org/10.1029/1999GL002330

Manalang, D., & Delaney, J. R. (2016). Axial Seamount—Restless, wired and occupied: A conceptual overview of resident AUV operations and technologies. Paper presented at *OCEANS 2016* MTS/IEEE, Monterey, CA. doi:https://doi.org/10.1109/OCEANS.2016.7761305

Massoth, G. J., Baker, E. T., Feely, R. A., Lupton, J. E., Collier, R. W., Gendron, J. F., et al. (1998). Manganese and iron in hydrothermal plumes resulting from the 1996 Gorda Ridge event. *Deep Sea Research, Part II*, *45*(12), 2683–2712. https://doi.org/10.1016/S0967-0645(98)00089-7

Massoth, G. J., Baker, E. T., Lupton, J. E., Feely, R. A., Butterfield, D. A., Von Damm, K., Roe, K. K., et al. (1994). Temporal and spatial variability of hydrothermal manganese and iron at Cleft segment, Juan de Fuca Ridge. *Journal of Geophysical Research*, *99*, 4905–4923. https://doi.org/10.1029/93JB02799

McDougall, T. J. (1990). Bulk properties of "hot smoker" plumes. *Earth and Planetary Science Letters*, *99*(1-2), 185–194. https://doi.org/10.1016/0012-821X(90)90081-8

McDuff, R. E. (1995). Physical dynamics of deep-sea hydrothermal plumes. In S. Humphris, et al. (Eds.), *Seafloor hydrothermal systems: Physical, chemical, biological, and geological interactions*, *Geophys. Monogr. Ser.*, (Vol. 91, pp. 357–368). Washington, D.C.: AGU.

McLaughlin-West, E. A., Olson, E. J., Lilley, M. D., Resing, J. A., Lupton, J. E., Baker, E. T., & Cowen, J. P. (1999). Variations in hydrothermal methane and hydrogen concentrations following the 1998 eruption at Axial Volcano. *Geophysical Research Letters*, *26*, 3453–3456. https://doi.org/10.1029/1999GL002336

Meyer, J. L., Akerman, N. H., Proskurowski, G., & Huber, J. A. (2013). Microbiological characterization of post-eruption "snowblower" vents at Axial Seamount, Juan de Fuca Ridge. *Frontiers in Microbiology*, *4*, 153. https://doi.org/10.3389/fmicb.2013.00153

Morton, B. R., Taylor, G. I., & Turner, J. S. (1956). Turbulent gravitational convection from maintained and instantaneous sources. *Proceedings of the Royal Society of London A*, *234*(1196), 1–23.

Nooner, S. L., & Chadwick, W. W. Jr. (2016). Inflation-predictable behavior and co-eruption deformation at Axial Seamount. *Science*, *354*(6318), 1399–1403. https://doi.org/10.1126/science.aah4666

Oosting, S. E., & Von Damm, K. L. (1996). Bromide/chloride fractionation in seafloor hydrothermal fluids from 9–10°N East Pacific Rise. *Earth and Planetary Science Letters*, *144*(1–2), 133–145. https://doi.org/10.1016/0012-821X(96)00149-5

Ramondenc, P., Germanovich, L. N., Von Damm, K. L., & Lowell, R. P. (2006). The first measurements of hydrothermal heat output at 9 50′ N, East Pacific Rise. *Earth and Planetary Science Letters*, *245*(3–4), 487–497. https://doi.org/10.1016/j.epsl.2006.03.023

Resing, J. A., Baker, E. T., Lupton, J. E., Walker, S. L., Butterfield, D. A., Massoth, G. J., & Nakamura, K.-I. (2009). Chemistry of hydrothermal plumes above submarine volcanoes of the Mariana Arc. *Geochemistry, Geophysics, Geosystems*, *10*, Q02009. https://doi.org/10.1029/2008GC002141

Resing, J. A., Feely, R. A., Massoth, G. J., & Baker, E. T. (1999). The water column chemical signature after the 1998 eruption of Axial Volcano. *Geophysical Research Letters*, *26*, 3645–3648. https://doi.org/10.1029/1999GL002350

Rona, P. A., & Trivett, D. A. (1992). Discrete and diffuse heat transfer at ASHES vent field, Axial Volcano, Juan de Fuca Ridge. *Earth and Planetary Science Letters*, *109*(1-2), 57–71. https://doi.org/10.1016/0012-821X(92)90074-6

Rubin, K. H., Soule, S. A., Chadwick, W. W. Jr., Fornari, D. J., Clague, D. A., Embley, R. W., et al. (2012). Volcanic eruptions in the deep sea. *Oceanography*, *25*(1), 142–157. https://doi.org/10.5670/oceanog.2012.12

Rudnicki, M. D., & Elderfield, H. (1992). Theory applied to the mid-Atlantic ridge hydrothermal plumes: The finite-difference approach. *Journal of Volcanology and Geothermal Research*, *50*(1–2), 161–172. https://doi.org/10.1016/0377-0273(92)90043-D

Spietz, R. L., Butterfield, D. A., Buck, N. J., Larson, B. I., Chadwick, W. W. Jr., Walker, S. L., et al. (2018). Deep-sea volcanic eruptions create unique chemical and biological linkages between the subsurface lithosphere and oceanic hydrosphere. *Oceanography*, *31*(1), 128–135. https://doi.org/10.5670/oceanog.2018.120

Turner, J. S. (1973). *Buoyancy effects in fluids*. Cambridge University Press. https://doi.org/10.1017/CBO9780511608827

Von Damm, K. L. (2004). Evolution of the hydrothermal system at East Pacific Rise 9°50′N: Geochemical evidence for changes in the upper oceanic crust. In C. R. German, J. Lin, & L. M. Parson (Eds.), *Mid-ocean ridges: Hydrothermal interactions between the lithosphere and oceans*, *Geophysical Monograph Series*, (Vol. 148, pp. 285–304). Washington, DC: American Geophysical Union. https://doi.org/10.1029/148GM12

Walker, S. L., Baker, E. T., Resing, J. A., Nakamura, K., & McLain, P. D. (2007). A new tool for detecting hydrothermal plumes: An ORP Sensor for the PMEL MAPR. *Eos, Transactions American Geophysical Union, 88*(52). Fall Meet. Suppl., Abstract V21D-0753.

Wilcock, W. S., Tolstoy, M., Waldhauser, F., Garcia, C., Tan, Y. J., Bohnenstiehl, D. R., et al. (2016). Seismic constraints on caldera dynamics from the 2015 Axial Seamount eruption. *Science*, *354*(6318), 1395–1399. https://doi.org/10.1126/science.aah5563

Wilcock, W. S. D., Dziak, R. P., Tolstoy, M., Chadwick, W. W. Jr., Nooner, S. L., Bohnenstiehl, D. R., et al. (2018). The recent volcanic history of Axial Seamount: Geophysical insights into past eruption dynamics with an eye toward enhanced observations of future eruptions. *Oceanography*, *31*(1), 114–123. https://doi.org/10.5670/oceanog.2018.117

Xu, G., & Lavelle, J. W. (2017). Circulation, hydrography, and transport over the summit of Axial Seamount, a deep volcano in the Northeast Pacific. *Journal of Geophysical Research: Oceans*, *122*, 5404–5422. https://doi.org/10.1002/2016JC012464

Yeo, I. A., Clague, D. A., Martin, J. F., Paduan, J. B., & Caress, D. W. (2013). Preeruptive flow focussing in dikes feeding historical pillow ridges on the Juan de Fuca and Gorda Ridges. *Geochemistry, Geophysics, Geosystems*, *14*, 3586–3599. https://doi.org/10.1002/ggge.20210